THE JOURNAL OF BIOLOGICAL CHEMISTRY VOL. 287, NO. 39, pp. 33026–33035, September 21, 2012

Base of the Measles Virus Fusion Trimer Head Receives the Signal That Triggers Membrane Fusion*[S]

Received for publication, April 17, 2012, and in revised form, July 27, 2012 Published, JBC Papers in Press, August 2, 2012, DOI 10.1074/jbc.M112.373308

Swapna Apte-Sengupta[‡], Surendra Negi[§], Vincent H. J. Leonard[‡], Numan Oezguen[§], Chanakha K. Navaratnarajah[‡], Werner Braun[§], and Roberto Cattaneo[‡1]

From the [‡]Department of Molecular Medicine, Mayo Clinic, and Virology and Gene Therapy Track, Mayo Graduate School, Rochester, Minnesota 55905 and the [§]Department of Biochemistry and Molecular Biology, and Sealy Center for Structural Biology and Molecular Biophysics, University of Texas Medical Branch, Galveston, Texas 77555

Background: A homology model of the trimeric measles virus fusion protein predicts a cavity in the base of the head.
Results: Hydrophobic residues required for interactions with the hemagglutinin map to this cavity.
Conclusion: The base of the measles virus fusion protein trimer head receives the signal that triggers membrane fusion.
Significance: Emerging, re-emerging, and prevalent paramyxoviruses may operate based on similar signal transmission mechanisms.

The measles virus (MV) fusion (F) protein trimer executes membrane fusion after receiving a signal elicited by receptor binding to the hemagglutinin (H) tetramer. Where and how this signal is received is understood neither for MV nor for other paramyxoviruses. Because only the prefusion structure of the parainfluenza virus 5 (PIV5) F-trimer is available, to study signal receipt by the MV F-trimer, we generated and energy-refined a homology model. We used two approaches to predict surface residues of the model interacting with other proteins. Both approaches measured interface propensity values for patches of residues. The second approach identified, in addition, individual residues based on the conservation of physical chemical properties among F-proteins. Altogether, about 50 candidate interactive residues were identified. Through iterative cycles of mutagenesis and functional analysis, we characterized six residues that are required specifically for signal transmission; their mutation interferes with fusion, although still allowing efficient F-protein processing and cell surface transport. One residue is located adjacent to the fusion peptide, four line a cavity in the base of the F-trimer head, while the sixth residue is located near this cavity. Hydrophobic interactions in the cavity sustain the fusion process and contacts with H. The cavity is flanked by two different subunits of the F-trimer. Tetrameric H-stalks may be lodged in apposed cavities of two F-trimers. Because these insights are based on a PIV5 homology model, the signal receipt mechanism may be conserved among paramyxoviruses.

Measles virus (MV),[2] an enveloped nonsegmented negative strand RNA virus, remains a significant public health problem (1). Although targeted for eradication (2), MV still caused 139,000 worldwide deaths in 2010 (3). In addition, relaxed vaccination discipline favored recent measles re-emergence in Europe and North America, now reporting small but costly epidemics (4, 5).

MV is a member of the family Paramyxoviridae that includes other deadly emerging viruses such as Hendra and Nipah and prevalent human pathogens such as mumps, parainfluenza, and respiratory syncytial viruses that still cause significant morbidity and mortality (6). Although many other enveloped viruses take advantage of low pH (7) or proteases (8) in the endosomal compartment to trigger membrane fusion, most paramyxoviruses including MV fuse directly with the plasma membrane (6, 9).

An accurate mechanism must be in place to secure timely and efficient MV cell entry at the plasma membrane. It is known that receptor binding to the attachment protein hemagglutinin (H) not only determines tropism (10, 11) but also contributes to fusion triggering.

MV H is a tetrameric type II transmembrane glycoprotein composed of an amino-terminal cytoplasmic tail, a membrane-spanning segment, and a membrane-proximal stalk region connected to a large cuboidal head contacting the receptors (12–14). Two H-heads are linked covalently at their base forming a homodimer (12), and two such dimers form a four-helix bundle tetrameric stalk (15). Although two forms of tetrameric interfaces were recently documented in crystals of shortened and mutated MV H-heads (16), it is unknown whether H-head dimers engage directly in tetrameric interactions when stabilized by the stalk.

Mechanisms of fusion triggering proposed for MV and the other paramyxoviruses focus on the interactions of the attachment protein stalks with the fusion (F) protein trimeric heads (9, 16–20). In particular, recent structural analyses of the ectodomain of the hemagglutinin-neuraminidase (HN) attachment protein not only revealed how the tetrameric stalk stabilizes two HN-head dimers (21), but also suggested that its central segment sustains signal transmission (21, 22). Analogously, the central segment of the H-stalk may sustain signal transmission (15).

* This work was supported, in whole or in part, by National Institutes of Health Grant R01-CA090636 (to R. C.).
[S] This article contains supplemental Fig. 1.
[1] To whom correspondence should be addressed: Mayo Clinic, Department of Molecular Medicine, 200 First St. SW, Rochester, MN 55905. E-mail: Cattaneo.Roberto@mayo.edu.
[2] The abbreviations used are: MV, measles virus; F, fusion protein; H, hemagglutinin; HN, hemagglutinin-neuraminidase; PIV5, parainfluenza virus 5.

However, how F-trimers receive the fusion-triggering signal is not understood. F-proteins are type I transmembrane glycoproteins whose ectodomain has a large globular head attached to a three-helix stalk (23). Their F_0 precursor is activated by proteolytic cleavage into a membrane-anchored F_1 and a disulfide-linked F_2 subunit (6). The hydrophobic amino terminus of F_1, which is named the fusion peptide, is wedged between two monomers near the equator of the prefusion trimer head structure. The only F-trimer prefusion structure available is that of parainfluenza virus 5 (PIV5) (23), but conserved cysteines in all paramyxoviral F-protein sequences facilitate their alignment and building of structural homology models.

Information about the arrangement of the glycoproteins in the MV envelope, although required to fully understand transmission of the triggering signal, is limited. Paramyxovirus particles analyzed by electron microscopy and negative staining can present spikes that extend 8–12 nm from the membrane bilayer (6), but one study has suggested that these structures may be formed only after unfolding and inactivation of F-trimers (24). Moreover, recent cryoelectron tomography analyses of MV particles documented an ~12-nm layer of strong density corresponding to the envelope glycoprotein ectodomains without revealing individual spikes (25). Interestingly, the H-stalk is 15–20 residues longer than the HN-stalk, and biochemical evidence suggested that the MV H-heads form a layer above F-trimers (26).

To characterize how MV F-trimers receive the fusion-triggering signal, we generated and energy-minimized a model based on the PIV5 prefusion F-trimer structure (23). We predicted potentially interacting patches on the MV F-trimer surface and considered individual amino acids based on their relative entropy in multiple F-protein sequence alignments (27). We assessed the function of many solvent-exposed residues and characterized six as signal transmission-relevant. Four of these residues line a large cavity in the base of the F-trimer head.

EXPERIMENTAL PROCEDURES

Template for Modeling—To identify the best template, the coding sequences of the MV F-protein (wild type strain IC323) (GI: AJ133108.1) (28) or vaccine-lineage strain NSe (29, 30) were defined as targets. This sequence differs only in two positions when compared with the wild type: M94V and G460W. These sequences were submitted to the metaserver GeneSilico (31), which distributed the query sequences into different fold recognition servers to identify the best template structure. Based on sequence identity and template score, we selected the PIV5 trimer crystal structure (Protein Data Bank (PDB): 2B9B) as the template for homology modeling.

Modeling the MV F-trimer Structure—The homology model was generated using procedures previously used for other proteins (32–34). Our modeling package MPACK combines the programs EXDIS (35), DIAMOD (36), and the energy minimization program FANTOM (37). The model structure was obtained by fitting the monomeric structure of the MV F-protein into the trimer structure of PIV5 and was energy-minimized in a water box with TIP3P water molecules for 10,000 iterations using NAMD (38) to remove steric clashes. Using PYMOL, the overall root mean square deviation values for the model and template were found to be 0.354 Å (FANTOM) and 0.878 Å (NAMD). The solvent-accessible surface area of amino acids was calculated using the program GETAREA (39).

Prediction of Interacting Residues with InterProSurf—Two approaches were used to predict residues on the surface of the MV F-trimer model involved in interactions with other proteins. The first approach, which was applied to the wild type F-protein, is based on InterProSurf, a method that identifies patches of potentially interacting amino acids in a protein complex using the three-dimensional structures of the individual subunits (40, 41). Using this method, amino acids on the MV F-trimer surface with solvent-accessible surface area greater than 10 $Å^2$ were distributed in 128 clusters. These clusters were ranked based on their InterProSurf scores (40) calculated from the propensity values of amino acids being in an interface and the solvent-accessible surface area of the amino acids in the three-dimensional model of the MV F-trimer. Amino acid residues from the top 40 clusters were selected. As the cluster decomposition was applied to the complete surface of the MV F-trimer and not separately to the individual monomers, some residues of high scoring clusters occurred less than three times in these top clusters. In the first mutagenesis round based on the wild type F-protein, we focused on those residues that occurred three times (frequency 3) in the top 40 list.

Combinatorial Prediction of Interacting Residues—A second mutagenesis approach was applied to the vaccine-lineage NSe F-protein sequence for diversification. It was based on the less restrictive criterion of frequency 2 or 3 in the InterProSurf analysis, in combination with conservation of residues in the Morbillivirus genus. Conservation was assessed with the PCPMer program suite, which defines conserved segments in aligned protein sequences according to high values of the relative entropy scale (42). The relative entropy values measure five quantitative descriptors of physical chemical properties of residues (43) in columns of a multiple sequence alignment relative to what would be expected if the amino acids in a column are randomly distributed. The relative entropy values are typically in the range of 1–2.5 for highly conserved positions and zero for a random distribution. We selected all positions in the MV F-protein sequence in the top half of the relative entropy values for the aligned sequences in the Morbillivirus genus. Nine F-protein sequences from the morbilliviruses were aligned: MV strains Schwarz (GenBank™: AAF85704.1) and AIK-C (GenBank: AAF85664.1); two variants of the canine distemper virus strain Onderstepoort (GenBank: CAA46481.1 and AAK54668.1); two variants of the rinderpest virus strain Kabete O (Swiss-Prot: P12574.1, and National Center for Biotechnology Information (NCBI): YP_087124.2); peste-des-petits-ruminants virus (GenBank: AAS68030.1); dolphin morbillivirus (NCBI: NP_945028.1); and phocine distemper virus (GenBank: BAA01206.1). Residues that were conserved in the broader Paramyxovirus family (morbilli, rubula, respiro, avula, henipa, and unclassified sequences) with high relative entropy were discarded as these residues are probably conserved for reasons different from the MV F-H interactions as heterotypic glycoproteins do not trigger fusion.

Cells—Human embryonic kidney 293 (HEK-293) (ATCC CRL-1573) cells were maintained in Dulbecco's modified

Eagle's medium (DMEM) supplemented with 10% fetal bovine serum (FBS) and 1% penicillin/streptomycin at 37 °C with 5% CO_2. Baby hamster kidney cells stably expressing the T7 polymerase (BHK-T7) (44) were maintained in DMEM supplemented with 10% FBS and 0.1 mg of G418/ml. Vero (ATCC CCL-81) and Vero/hSLAM (Vero cells stably expressing human signaling lymphocyte activation molecules (kindly provided by Y. Yanagi)) (45) were maintained in DMEM supplemented with 10% FBS and 0.5 mg of G418/ml. Chinese hamster ovary (CHO) cells (ATCC CCL-61) were maintained in DMEM supplemented with 10% FBS and 0.5 mg of nonessential amino acids/ml.

Expression Plasmids and Mutagenesis—All the F-protein mutants were generated in pCG-F Wt and pCG-F vaccine lineage strain plasmids (29) by QuikChange site-directed mutagenesis (Stratagene, La Jolla, CA). The integrity of each clone was confirmed by sequencing the entire F-protein gene.

Antibodies—Polyclonal antiserum (F_{cyt}) to a peptide mimicking a region in the cytoplasmic tail of MV F and antiserum (H_{cyt}) to a peptide in the cytoplasmic tail of H-protein (46) were raised in rabbits; conformation-sensitive monoclonal antibodies cl55 (anti-H) and Y503 (anti-F) were kind gifts from Dr. Gerlier, INSERM, Lyon, France. Monoclonal anti-MV F antibody 186CA (47) was a kind gift from Branka Horvat, INSERM (Lyon, France), and 19GD6 (48) was a kind gift from Mariethe Ehnlund, Karolinska Institute, Stockholm, Sweden. HRP-conjugated goat anti-mouse (Pierce) and phycoerythrin-conjugated goat anti-mouse (Jackson ImmunoResearch, West Grove, PA) antibodies were obtained commercially.

Fusion Assays—Vero/hSLAM cells were seeded onto 24-well plates 12 h before transfection. Transfection was done by diluting 7.5 μl of Lipofectamine 2000^{TM} (Invitrogen) in 50 μl of Opti-MEM followed by incubation for 10 min. Meanwhile, 1 μg wild type or mutant F-plasmid DNA, 1 μg of wild type H-plasmid, and 1 μg of enhanced GFP plasmid DNA were diluted in 50 μl of Opti-MEM. The two solutions were combined and incubated for 20 min at room temperature. The transfection mixture was overlaid onto the cells, and fusion was monitored 16 h after transfection by observing the syncytia under the microscope. The extent of fusion in one field of view (about 2000 cells) was recorded by using the following meter: 0, two or fewer 4–5-nuclei syncytia (background); 1, three or more 4–5-nuclei syncytia; 2, one to three syncytia with more than 10 nuclei; 3, four or more syncytia with more than 10 nuclei.

Quantitative Fusion Assays—BHK-T7 cells were seeded onto a 24-well plate (1×10^5 cells/well) and transfected with 0.5 μg of wild type or mutant F-plasmids and 0.5 μg of wild type H-plasmid with Lipofectamine 2000 (Invitrogen). Vero/hSLAM cells were seeded onto a 6-well plate (6×10^5 cells/well) and transfected with 1.4 μg (per well) of pTM1-luc, a plasmid expressing a T7-driven luciferase reporter gene. Six hours after transfection, the Vero/h/SLAM cells were washed and detached by Versene (Invitrogen) treatment and overlaid onto the BHK-T7 cells. After 8 h, the expression of luciferase was quantified by incubating the cells with Steady-Glo (Promega, Madison, WI) for 5 min at room temperature and reading the emission on a Topcount-NXT luminometer (Packard, Los Angeles, CA).

Immunoblots—HEK-293 cells were seeded onto 6-well plates 12 h before transfection. At ~80% confluence, the cells were transfected with 2 μg of plasmid DNA with 5 μl of Lipofectamine 2000. After 36 h of transfection, the cells were lysed in radioimmune precipitation buffer (50 mM Tris, pH 8.0, 62.5 mM EDTA, 0.4% deoxycholate, 1% IGEPAL, and 1 mM phenylmethylsulfonyl fluoride (PMSF)), cleared by centrifugation at 12,000 rpm for 10 min at 4 °C, and boiled with urea buffer (200 mM Tris, pH 6.8, 8 M urea, 5% SDS, 0.1 mM EDTA, 0.03% bromphenol blue, and 1.5% DTT) for 5 min. The protein samples were resolved on 4–15% gradient SDS-polyacrylamide gel, transferred to polyvinylidene difluoride membranes (PVDF) (Millipore, Billerica, MA), probed with monoclonal rabbit anti-F_{cyt} or anti-H_{cyt} antibodies, and visualized by ECL plus reagent (GE Healthcare).

Co-immunoprecipitation—Forty hours after transfection cells were washed in PBS twice and lysed by three freeze-thaw cycles in PBS supplemented with protease inhibitors and 1 mM PMSF. The lysates were cleared by centrifugation and, the supernatants were incubated with antibody cl55 and 25 μl of protein G-agarose beads at 4 °C for 2 h. The beads were pulled down, washed with PBS twice, and resuspended in urea buffer. The samples were boiled for 5 min and subjected to immunoblots using the anti-F_{cyt} antibody. Protein bands were quantified using the Typhoon fluorimager (GE Healthcare) and the ImageQuant 5.0 software (Molecular Dynamics).

Cell Surface Expression Analysis by Flow Cytometry—Vero/hSLAM or CHO cells were transfected with F- and H-plasmid DNAs as described above. The cells were detached by incubating with Versene (Invitrogen) for 10 min at room temperature, washed twice in cold FACS washing buffer (1× PBS, 2% FBS, 0.1% NaN_3), and exposed to various temperatures (37, 45, 55, and 65 °C) for 10 min when necessary. The cells were then incubated with primary antibody (1:1000 dilution) for 1 h at 4 °C. After three washes in the FACS washing buffer, the cells were incubated with secondary antibody conjugated with phycoerythrin (1:500 dilutions) for 1 h at 4 °C. The cells were washed and fixed in 4% paraformaldehyde and read by FACSCalibur (BD Biosciences). The results were analyzed by FlowJo software (Tree Star Inc., Ashland, OR).

RESULTS

New MV F-trimer Model and Its Use to Guide Mutagenesis—In the absence of structural information on the MV F-trimer, we modeled it based on the crystal structure for the prefusion form of the PIV5 F-trimer (Fig. 1 and "Experimental Procedures"). The model was energy-minimized and used to predict surface residues likely to interact with other proteins.

We used two complementary approaches to predict interacting amino acids. One was based on the InterProSurf program (41) that identifies potentially interacting clusters of residues (Fig. 1*B*, *bottom right*, *salmon color*). The other used, in addition, the conservation level of individual amino acids, which was measured using the PCPMer program (27). The approaches yielded two overlapping sets of candidate residues as listed in Fig. 2*A*. The combination analysis yielded 39 candidates (*left columns*), whereas InterProSurf alone yielded 33 candidates (*right columns*). Of the total 49 candidates, 23 were

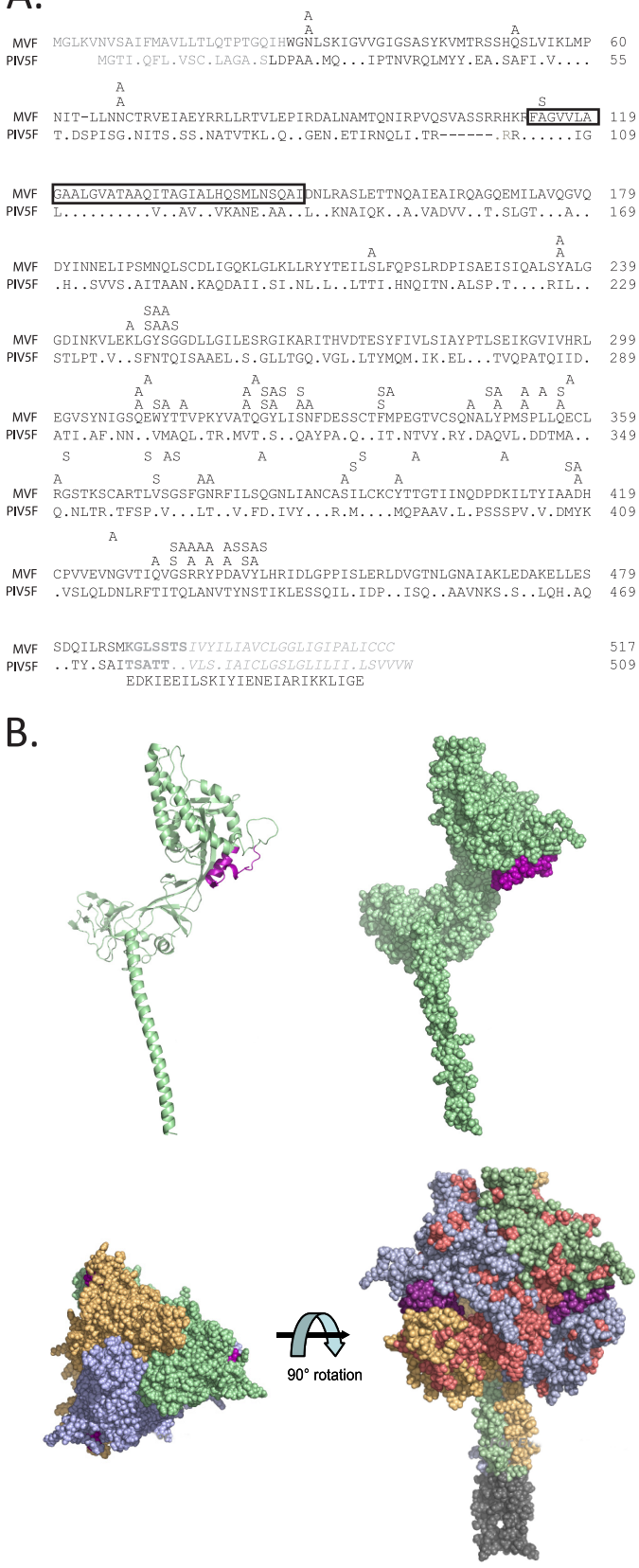

FIGURE 1. **Alignment of the sequences of MV and PIV5 ectodomains and structural model of the MV F-trimer.** *A*, *MVF*, sequence of the F-protein of the MV IC-B strain. *PIV5F*, sequence of the F-protein of PIV5. Positions identical with MVF are indicated with a *dot*. The signal peptides at the amino terminus and the transmembrane domain near the carboxyl terminus are shown in *gray*. The membrane-proximal 7-residue external region (MPER) (52) is shown in *bold gray*, and a *box* is drawn around the predicted MV fusion peptide. The single gap introduced in the MVF sequence and the one in the PIV5F sequence are shown with *dashes*. The GCNt sequence used to stabilize PIV5F is shown in the line immediately below the PIV5F sequence. The position and nature of the 83 single amino acid mutations introduced for this study are indicated in the three lines above the MVF sequence. *Line immediately above F*, substitutions introduced in the vaccine lineage strain. *Middle line*, substitutions in the wild type strain (first mutagenesis round). *Top line*, additional substitutions introduced around anchor residues (second mutagenesis round). *B*, F-protein structural model. *Top*, backbone (*left*) and surface (*right*) representations of one MV F-monomer. *Bottom*, top (*left*) and side (*right*) view of an F-trimer. The three subunits are shown in *light orange*, *light blue*, and *pale green*. The fusion peptide is shown in *purple*, and the top 40 surface cluster residues are shown in *salmon*. The GCNt trimer stabilizing region used to mimic the transmembrane region is shown in *gray*.

predicted by both strategies. In consideration of the significant overlap of the two sets of mutants, mutagenesis was executed in two different backbones, vaccine lineage or wild type. These F-protein backbones differ in two residues ("Experimental Procedures"), and the vaccine lineage protein is slightly more fusogenic than the wild type.

Mutagenesis was based on two small amino acids: alanine to substitute charged and polar residues and serine to replace apolar residues. These residues were chosen to limit structural interference possibly leading to reduced protein folding and transport.

Identification of F-residues Sustaining Efficient Fusion—The function of each F-protein mutant was assessed by documenting the level of syncytia formation after co-transfection of the corresponding F-expression plasmid with the standard H-protein expression plasmid. Fig. 2*A* documents the different levels of fusion (0-1-2-3) for controls and two mutants. Although most of the 72 mutants tested fully retained their fusion function, 29 lost different levels of functional competence (Fig. 2*B*). Because we were interested in mutants with strong effects, we focused on those eight that lost more than 50% of their function. This level was defined by either the average of the results with both backbones or the average of the results on the only backbone tested.

Analysis of protein expression for these mutants (Fig. 3*A*) revealed that L325S, Y349A, and R360A (Fig. 3*B*, *red*) were processed efficiently, whereas W311A, L348S, I393S, D418A, and Y437A (Fig. 3*B*, *blue*) were processed inefficiently if at all. Remarkably, all these mutants are located in the lower half of the F-trimer head and form a belt below the fusion peptide (Fig. 3*B*, *purple*). All mutants located above the fusion peptide retained most or all of their function (Fig. 3*B*, *white residues*).

The eight residues with greatly reduced fusion function served as starting points (anchors) for the next round of mutagenesis, which included all solvent-exposed amino acids near which α-carbon atoms are predicted to be located within 10 Å of those of the anchor residues. These criteria identified 11 additional residues, shown in *orange* on the F-trimer model (Fig. 3*B*). The corresponding proteins were expressed, and their function and processing were documented.

Fig. 4*A* shows a gel analysis of protein processing, with the average results of multiple fusion assays indicated above each lane. Mutants E310A, G361S, and T400A did not induce fusion and were not processed into F_1 and F_2 (*blue boxes* above the

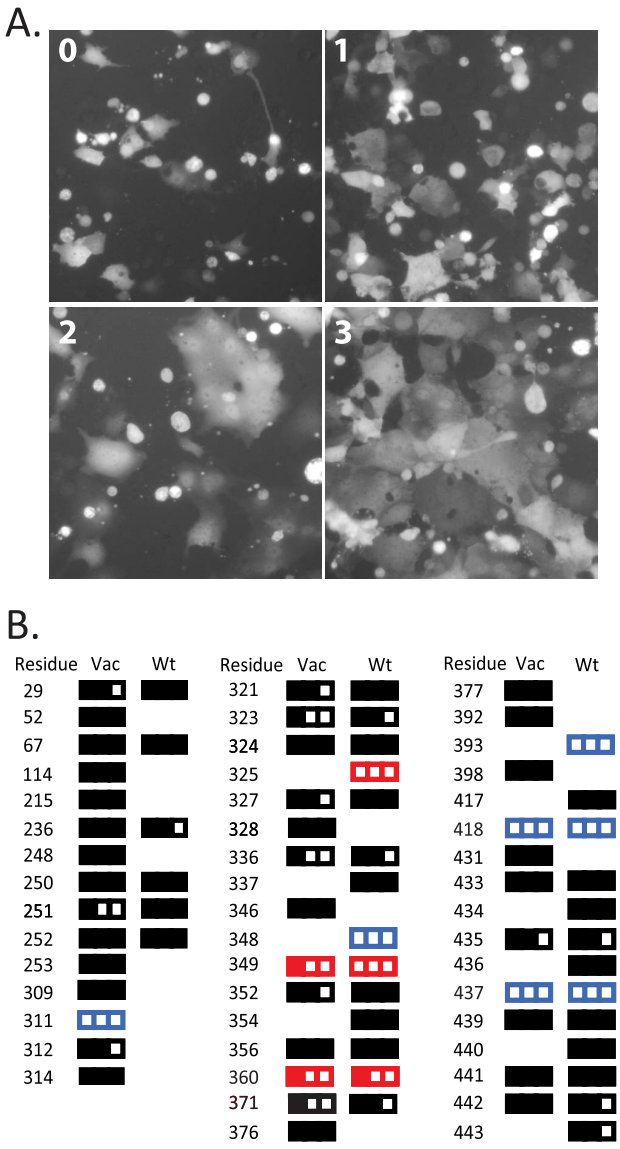

FIGURE 2. **Fusion efficiency of first round F-protein mutants.** *A*, syncytium formation in Vero/hSLAM cells after F- and H-protein coexpression. Cells were photographed 24 h after transfection. *Level 0*: negative control, H-expression plasmid alone. *Level 1*: mutant R360A. *Level 2*: mutant V371S. *Level 3*: positive control, wild type F. *B*, residues mutated in a vaccine lineage (*Vac*) or a wild type (*Wt*) backbone. The results of the fusion assay for each mutant (average of at least three assays) are indicated with *rectangles*. A *full rectangle* indicates full fusion activity, a *void rectangle* indicates no fusion activity, and *two-thirds-* and *one-third-filled rectangles* indicate intermediate fusion level, as defined under "Experimental Procedures." Color qualifies the processing characteristics of the mutants with low fusion function; *red* indicates efficient processing into F_1, and *blue* indicates minimal or no processing of F_0.

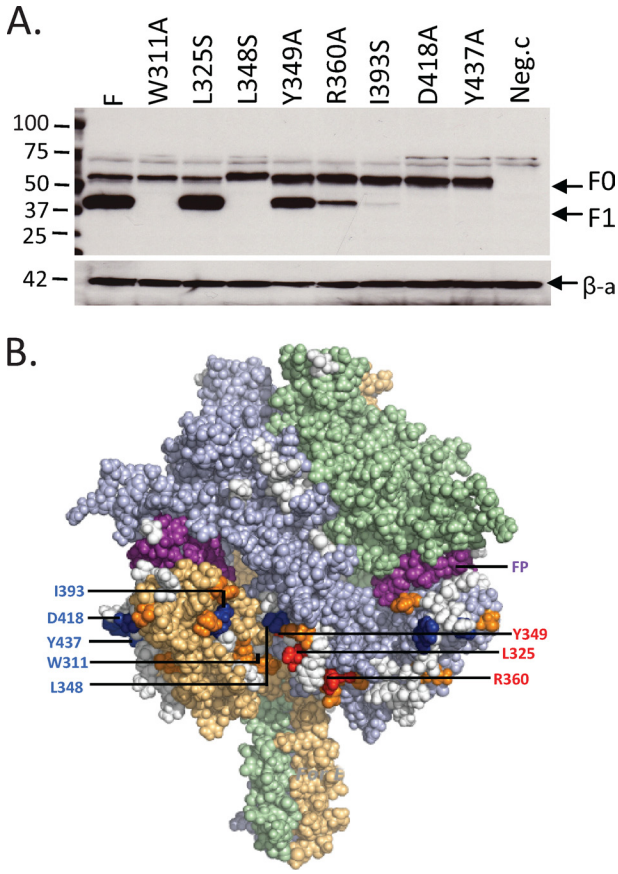

FIGURE 3. **Processing of the first round F-protein mutants with strongly impaired function and their localization on the F-trimer model.** *A*, protein extracts from cells used for one of the functional assays were separated on a gel, and the F-proteins (*top panel*) or β-actin (*bottom panel*, loading control) were characterized by immunoblot. Mutant identity is indicated above each lane. F-processing analyses that were done in absence of H yielded equivalent results (not shown). Molecular mass marker sizes are indicated on the *left*. *F*, standard F-protein; *Neg.c*, empty vector (negative control). The positions of the unprocessed (F_0) and processed (F_1) protein bands are indicated on the *right*. *β-a*, β-actin. *B*, localization of the residues affecting fusion function and processing of the F-protein. The fusion peptide is colored *purple*; the eight anchor residues are colored either *red* or *blue* according to the convention above. The surface residues surrounding the anchors within 10 Å distance are colored *orange*. Residues whose modification did not strongly affect membrane fusion are shown in *white*.

corresponding lanes). Mutants Q322A, Q383A, and L394S did not induce fusion but were processed at levels close to wild type (*red boxes* above the corresponding lanes). The other five mutants retained significant fusion function.

Thus, a total of 14 residues required for fusion function were identified. Six of the corresponding proteins (Fig. 4*B*, *red residues*) were efficiently processed into F_1 and F_2, whereas the other eight (Fig. 4*B*, *blue residues*) were not. We further confirmed the fusion function of these six efficiently processed mutants using a quantitative fusion assay (17) that uses a luciferase reporter to monitor the extent of fusion.

Fig. 5 documents the levels of luciferase expression recorded for each mutant, confirming that their fusion function is less than 50% of that of the wild type F-protein. In particular, the three mutants with fusion level 1 in the semiquantitative assay (Q322A, R360A, and Q383A) retained about 20–40% of fusion function, whereas the other three mutants with fusion level 0 were only marginally if at all above background. We then analyzed cell surface expression of the six correctly processed proteins and documented that five are expressed at levels similar (60–140%) to standard F (supplemental Fig. 1), whereas R360A is expressed at about 3-fold reduced levels.

Hydrophobic Interactions Are Important for Fusion—Three of the six amino acids required specifically for signal transmission, Leu-325, Tyr-349, and Leu-394, have hydrophobic side chains. To test whether hydrophobicity is important for function, we mutated the corresponding side chains, introducing a charged residue, either aspartate or lysine. Conservative mutations to valine or tryptophan were also introduced as controls.

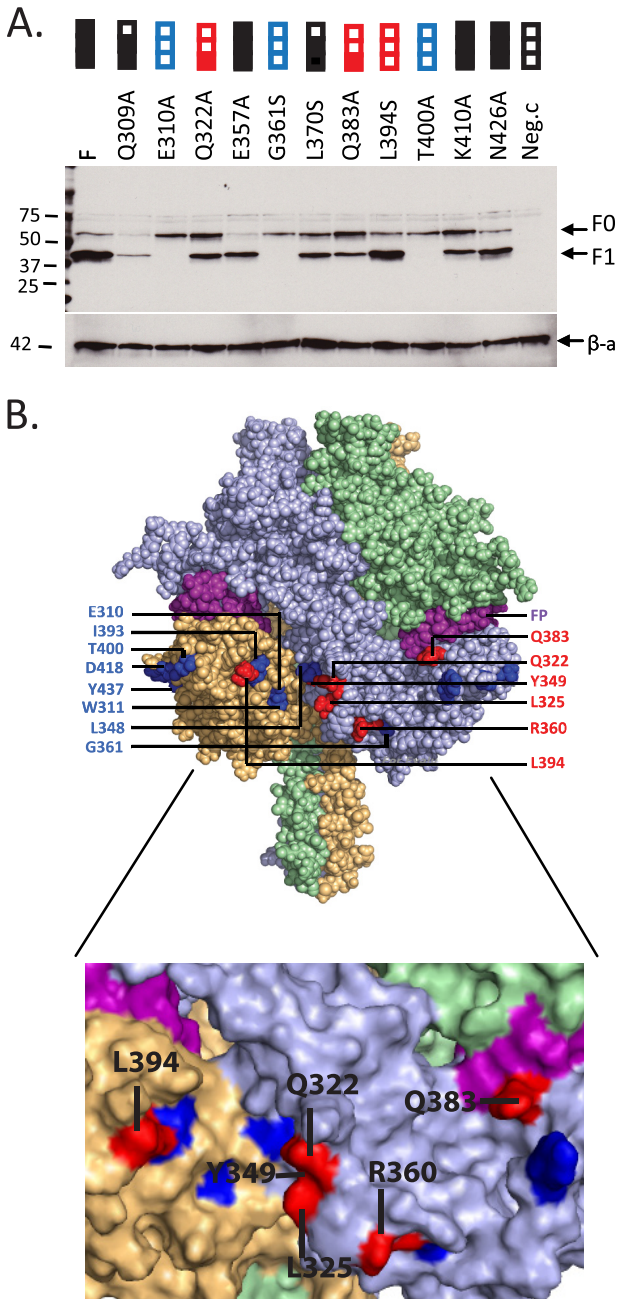

FIGURE 4. **Processing and function of the second round F-protein mutants and their localization on the F-trimer model.** *A*, protein extracts from transfected cells were separated on a gel, and the F-proteins were characterized by immunoblot. Mutant identity is indicated above each lane. Molecular mass marker sizes are indicated on the *left*. Results of the fusion assays performed before cell lysis are indicated above each lane with the same conventions used in Fig. 2. *F*, standard F-protein; *Neg.c*, empty vector. The positions of the unprocessed (F_0) and processed (F_1) protein bands are indicated on the *right*. *β-a*, β-actin. *B*, localization of the mutants on the F-trimer model, surface representation. *Inset*: portion of the F-trimer where most of the important residues are located. Color coding is as in Fig. 3.

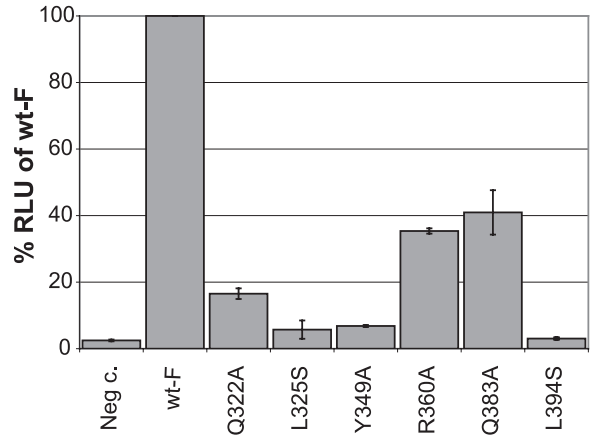

FIGURE 5. **Quantitative analysis of the fusion function of the six key F-protein mutants.** A quantitative fusion assay was performed 14 h after transfection. Mutants are indicated on the horizontal axis. *Neg c.*, negative control (H-protein expression plasmid only). *Wt-F*, positive control (standard F-protein expression plasmid). The vertical axis indicates relative luciferase units (*RLU*) presented as a percentage of Wt-F. Results represent the average of three replicates; *error bars* indicate the S.D.

We documented the efficiencies with which the mutated F-proteins executed membrane fusion. Although the proteins with control hydrophobic residues were functional, all charged substitutions abolished fusion (Fig. 6*A*, *top three rows*, *left* and *center panels*). We then characterized processing of the mutant proteins. Except Y349D, which was not processed, all the other proteins were processed with efficiency similar to wild type (Fig. 6*B*).

We also measured thermal stability of the three mutant F-proteins that revealed the involvement of hydrophobic side chains in the interactions with H. For this we took advantage of the pair of antibodies 186CA and 19GD6 (47, 48), which recognize the prefusion and the triggered F forms, respectively.[3]

Fig. 7 documents the reactivity of wild type F and of the L325S, L394S, and Y349A mutants with 186CA, recognizing the prefusion conformation (*top panel*), and with 19GD6, recognizing the triggered conformation (*bottom panel*). Although wild type F and the L325S and L394S mutants exhibited equivalent stability, mutant Y349A was slightly more stable, maintaining reactivity to the former antibody even after incubation at 55 °C. Altogether, these experiments show that a hydrophobic environment is important for the fusion process and that the mutations considered here do not simply destabilize the corresponding F-mutants.

Three F-mutants Have Reduced Interactions with H—We then asked whether the six F-protein mutants (Q322A, L325S, Y349A, R360A, Q383A, and L394S) that retained processing into F_1 and F_2 also retained efficient interactions with the H-protein by assessing whether they co-immunoprecipitate. Fig. 8*A* shows the primary data of one co-immunoprecipitation analysis, and Fig. 8*B* shows the primary data of the control experiments documenting protein expression levels. In addition, Fig. 8*C* shows the average and standard deviation of four co-immunoprecipitation analyses, and Fig. 8*D* shows the corresponding total protein expression controls.

The results can be summarized as follows. Proteins Q322A and L325S co-immunoprecipitated with an efficiency equivalent to that of wild type F, whereas proteins Y349A, Q383A, and L394S had 35–50% reduced efficiency. Co-immunoprecipitation of R360A was also reduced, but this protein was

[3] P. Plattet, personal communication.

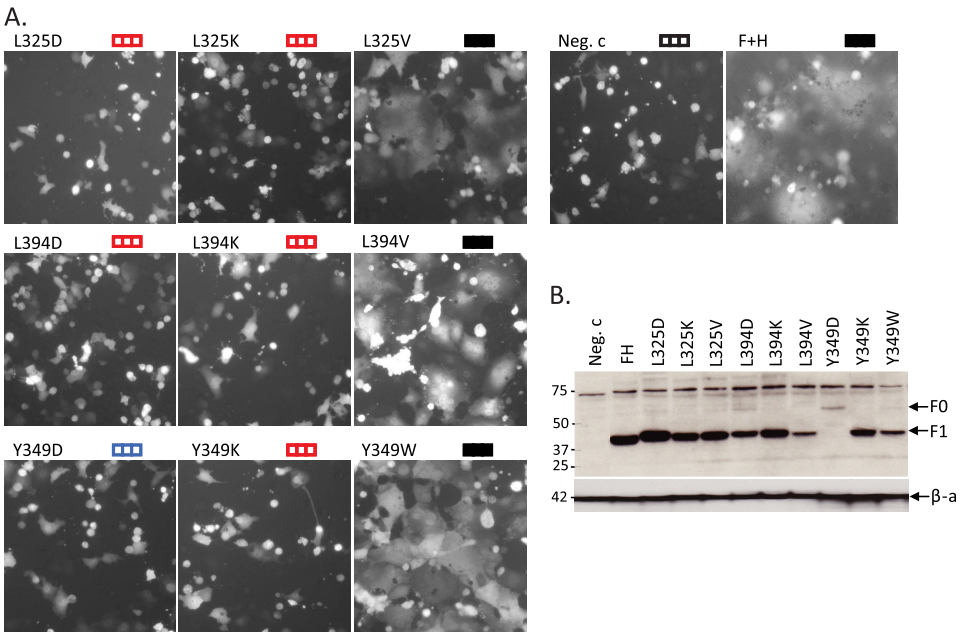

FIGURE 6. **Hydrophobic nature of three residues is important for fusion function.** *A*, extent of cell fusion supported by F-protein mutants. Cells were co-transfected with the F-expression plasmid indicated, an H-expression plasmid, and a GFP-expression plasmid, and the extent of syncytia formation was documented. Conventions used to indicate extent of fusion are as in Fig. 2. *Neg.c*, empty vector. *B*, F-protein expression and processing. Protein extracts from cells used for the functional assays of *panel A* were separated on a gel, and the F-proteins were characterized by immunoblot. Mutant identity is indicated above each lane. *FH*, wild type F and H expression (positive control). The positions of the unprocessed (F_0) and processed (F_1) protein bands are indicated on the *right*. *β-a*, β-actin.

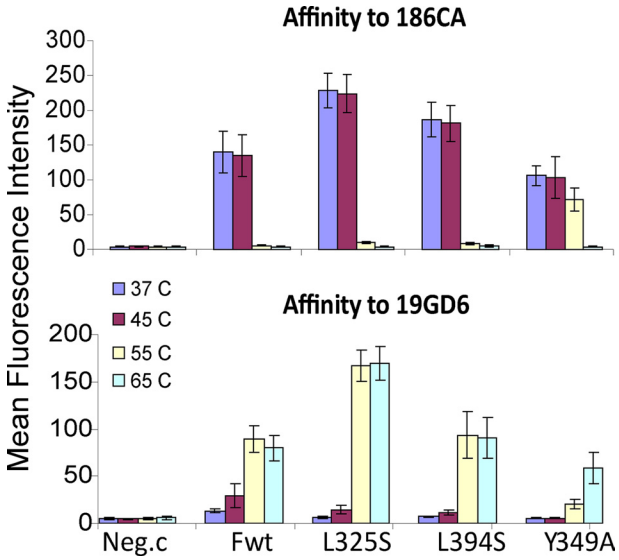

FIGURE 7. **Thermal stability of three F-protein mutants.** Cells expressing the proteins indicated at the bottom were exposed to the temperatures indicated on the *left* for 10 min, fixed, stained, and sorted. *Fwt*, standard F-protein. *Neg.c*, empty plasmid. F-protein on the cell surface was detected with conformation-specific antibodies 186CA (*top panel*) or 19GD6 (*bottom panel*); fluorescence intensity of individual cells was measured by FACS. The vertical axis indicates mean fluorescence intensity. Mean and standard deviations are indicated on each column. Color coding for temperature exposure is on the *left*.

expressed at lower levels; in experiments with this mutant, reduced H-protein levels were also consistently documented. Thus, these six F-protein mutations had limited or no effect on the interactions with H when introduced individually, suggesting that multiple interactions stabilize F-H oligomer complexes.

DISCUSSION

Decisive interactions for viral tropism occur at cell entry. After binding specific receptors, paramyxoviruses including MV fuse their envelope with the plasma membrane at neutral pH. Transmission of the membrane fusion triggering signal involves opening of the dimeric interface of the H-heads (17), followed by conformational changes of a central segment of the H-stalk (15). We focused here on signal receipt by the F-trimer and identified six residues, all located in the lower half of the F-trimer head. Although one of these residues (Gln-383) is adjacent to the fusion peptide, the other five cluster inside or near a large cavity in the base of the head. This cavity is flanked by two different subunits of the F-trimer.

In Fig. 4*B*, the *lower panel* presents a close-up of the inter-subunit cavity; four residues form a half circle within it. From the left, Leu-394 is located on the left side of the cavity in one monomer (*yellow shading*); Tyr-349 is located at the back of the cavity; and contiguous residues Gln-322 and Leu-325 are located on the right side. These three residues are contributed by another monomer (*light blue shading*). Arg-360 is a charged residue located to the right of Leu-325, but outside the cavity. The distance between the α-carbon atoms of Gln-322 and Leu-394 is ~21 Å, whereas the widest distance between the α-carbon atoms of the two helices of the four-helix bundle HN-protein stalk is ~18 Å. Thus, two helices of the H-stalk could fit in the cavity.

As to the F-H contacts, because these lateral cavities are open toward the top and the F-head is convex, the upper part of the H-stalk may not clash with it. Moreover, the H-stalk, which is 15–20 residues longer than the HN-stalk, would locate the H-head layer above the F-trimer layer (26). We note that two different arrangements on the stalk have been considered: first,

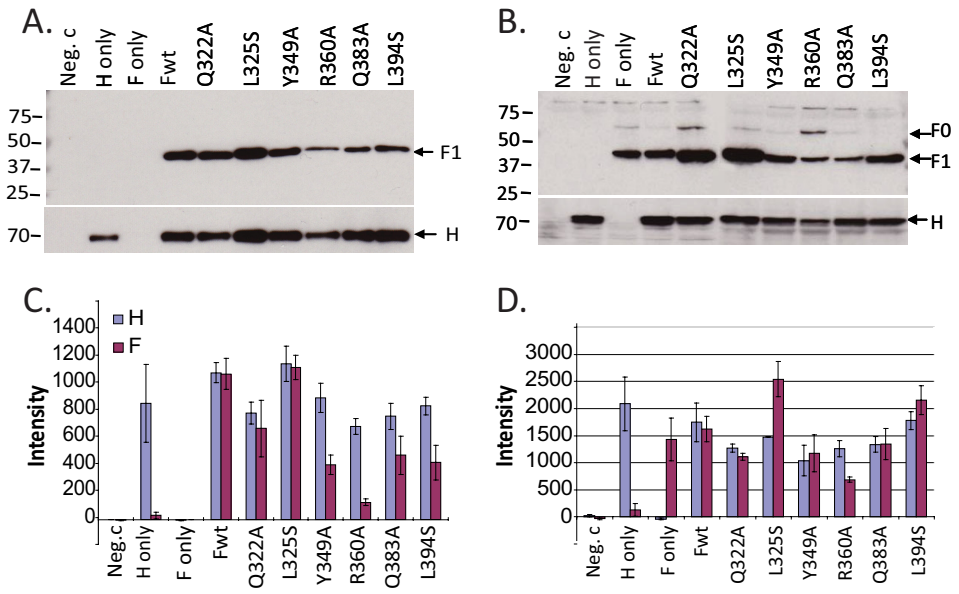

FIGURE 8. **Co-immunoprecipitation analyses of the interactions of the F-protein mutants with H.** Cells were transfected with the plasmids indicated above the gels or below the columns. *A* and *B*, individual experiments: co-immunoprecipitations and total cell lysates, respectively. The first three lanes are controls: *Neg.c*, empty plasmid; *H only* and *F only*, these plasmids alone. In the next seven lanes, standard F-protein (*Fwt*) or the six mutants indicated were co-transfected with standard H. For immunoprecipitation, the anti-H antibody cl55 was used. Precipitated complexes were separated on a PVDF membrane and probed with anti-F_{cyt} (*top panels*) or anti-H_{cyt} (*bottom panels*) antibodies. Molecular mass marker sizes are indicated on the *left*, and the positions of the F- and H-proteins are indicates on the *right*. *C* and *D*, graphic summaries of the quantitative results of four experiments. Protein bands were quantified using the Typhoon fluorimager and the Imagequant 5.0 software; *y*-axes indicate pixel intensities of the protein bands. *Error bars* indicate the S.D.

"heads-up," with heads located on the top of the stalk, possibly making tetrameric contacts similar to those observed in crystal structures derived from incomplete H-heads missing their stalks and stalk-proximal segment (16); and second, "heads-down," as revealed by the crystal structure of HN-heads with their tetrameric stalk, in which head-dimers adhere laterally to the stalk, without making direct tetrameric contacts (21). Although we do not know whether the MV H-heads are arranged "up" or "down" on the viral surface, both arrangements are compatible with tetrameric H-stalks being lodged in apposed cavities of two F-trimers.

Do F-trimers of other paramyxoviruses receive the triggering signal through an analogous mechanism? Studies based on segment exchanges between the F-proteins of human parainfluenza virus 2 and simian virus 41 did identify segments possibly involved in contacts, but these analyses have not been refined at the amino acid level (51). Nevertheless, because our study is based on a homology model, the signal transmission mechanism considered here may be conserved among paramyxoviruses, including those that cause lethal disease such as Nipah and Hendra and prevalent human pathogens such as mumps and human respiratory syncytial virus.

Other F-protein residues have been shown to affect function. A comparative analysis of fusion efficiency based on differences between two MV strains concluded that Phe in place of Leu at position 278 results in more efficient fusion (49). Residue 278 is part of the hydrophobic core of the protein, and it is conceivable that a large aromatic side chain slightly destabilizes the F-trimer, promoting more efficient fusion.

Another analysis focused on four residues differing between the F-proteins of two strains of the morbillivirus canine distemper virus (50). This analysis concluded that the residues homologous to MV Ala-121 and Lys-205 are determinants of physical glycoprotein interactions (50). Because Lys-205 is buried in the trimer, near the top of the head, an indirect effect was considered. For Ala-121, which is part of the fusion peptide, a direct effect was proposed (50). However, in view of the data presented here, even for Ala-121, an indirect effect on the interaction with H appears more likely.

In summary, molecular modeling predicted the existence of a large cavity in the base of the MV F-trimer head. Functional studies characterized this cavity as a site required for receiving the fusion-triggering signal. Biochemical analyses indicated that hydrophobic interactions in the cavity are important for signal transmission. We are considering the hypothesis that tetrameric H-stalks fit between two apposed F-trimers. To challenge this hypothesis, we are generating docking models predicting how the side chains of individual residues in F-trimers and tetrameric H-stalks engage. We will then introduce compensating mutations on both sides to reconstitute function.

Acknowledgments—We are grateful to Yusuke Yanagi for Vero/hSLAM cells, Denis Gerlier for cl55 and Y503 antibodies, Branka Horvat for 186CA antibody, and Mariethe Ehnlund for 19GD6 antibody. We also thank Philippe Plattet for helpful discussions.

REFERENCES

1. Griffin, D. E. (2007) Measles Virus. in *Fields' Virology, Fifth Edition* (Fields, B., Knipe, D. M., and Howley, P. M. eds.) pp. 1551–1585, Lippincott Williams and Wilkins, Philadelphia
2. Moss, W. J. (2009) Measles control and the prospect of eradication. *Curr. Top. Microbiol. Immunol.* **330,** 173–189
3. (2011) Vaccines: The case of measles. *Nature* **473,** 434–435

4. Chen, S. Y., Anderson, S., Kutty, P. K., Lugo, F., McDonald, M., Rota, P. A., Ortega-Sanchez, I. R., Komatsu, K., Armstrong, G. L., Sunenshine, R., and Seward, J. F. (2011) Health care-associated measles outbreak in the United States after an importation: challenges and economic impact. *J. Infect. Dis.* **203,** 1517–1525
5. Kupferschmidt, K. (2012) Public health: Europe's embarrassing problem. *Science* **336,** 406–407
6. Lamb, R. A., and Parks, G. D. (2007) Paramyxovirus: The viruses and their replication. in *Fields' Virology*, Fifth Ed. (Fields, B., Knipe, D. M., and Howley, P. M., eds) pp. 1305–1340, Lippincott Williams and Wilkins, Philadelphia
7. Marsh, M., and Helenius, A. (2006) Virus entry: open sesame. *Cell* **124,** 729–740
8. Chandran, K., Sullivan, N. J., Felbor, U., Whelan, S. P., and Cunningham, J. M. (2005) Endosomal proteolysis of the Ebola virus glycoprotein is necessary for infection. *Science* **308,** 1643–1645
9. Iorio, R. M., Melanson, V. R., and Mahon, P. J. (2009) Glycoprotein interactions in paramyxovirus fusion. *Future Virol.* **4,** 335–351
10. Mühlebach, M. D., Mateo, M., Sinn, P. L., Prüfer, S., Uhlig, K. M., Leonard, V. H., Navaratnarajah, C. K., Frenzke, M., Wong, X. X., Sawatsky, B., Ramachandran, S., McCray, P. B., Jr., Cichutek, K., von Messling, V., Lopez, M., and Cattaneo, R. (2011) Adherens junction protein nectin-4 is the epithelial receptor for measles virus. *Nature* **480,** 530–533
11. Tatsuo, H., Ono, N., Tanaka, K., and Yanagi, Y. (2000) SLAM (CDw150) is a cellular receptor for measles virus. *Nature* **406,** 893–897
12. Hashiguchi, T., Kajikawa, M., Maita, N., Takeda, M., Kuroki, K., Sasaki, K., Kohda, D., Yanagi, Y., and Maenaka, K. (2007) Crystal structure of measles virus hemagglutinin provides insight into effective vaccines. *Proc. Natl. Acad. Sci. U.S.A.* **104,** 19535–19540
13. Navaratnarajah, C. K., Vongpunsawad, S., Oezguen, N., Stehle, T., Braun, W., Hashiguchi, T., Maenaka, K., Yanagi, Y., and Cattaneo, R. (2008) Dynamic interaction of the measles virus hemagglutinin with its receptor signaling lymphocytic activation molecule (SLAM, CD150). *J. Biol. Chem.* **283,** 11763–11771
14. Brindley, M. A., and Plemper, R. K. (2010) Blue native PAGE and biomolecular complementation reveal a tetrameric or higher-order oligomer organization of the physiological measles virus attachment protein H. *J. Virol.* **84,** 12174–12184
15. Ader, N., Brindley, M. A., Avila, M., Origgi, F. C., Langedijk, J. P., Örvell, C., Vandevelde, M., Zurbriggen, A., Plemper, R. K., and Plattet, P. (2012) Structural rearrangements of the central region of the morbillivirus attachment protein stalk domain trigger F-protein refolding for membrane fusion. *J. Biol. Chem.* **287,** 16324–16334
16. Hashiguchi, T., Ose, T., Kubota, M., Maita, N., Kamishikiryo, J., Maenaka, K., and Yanagi, Y. (2011) Structure of the measles virus hemagglutinin bound to its cellular receptor SLAM. *Nat. Struct. Mol. Biol.* **18,** 135–141
17. Navaratnarajah, C. K., Oezguen, N., Rupp, L., Kay, L., Leonard, V. H., Braun, W., and Cattaneo, R. (2011) The heads of the measles virus attachment protein move to transmit the fusion-triggering signal. *Nat. Struct. Mol. Biol.* **18,** 128–134
18. Connolly, S. A., Leser, G. P., Jardetzky, T. S., and Lamb, R. A. (2009) Bimolecular complementation of paramyxovirus fusion and hemagglutinin-neuraminidase proteins enhances fusion: implications for the mechanism of fusion triggering. *J. Virol.* **83,** 10857–10868
19. Mirza, A. M., Aguilar, H. C., Zhu, Q., Mahon, P. J., Rota, P. A., Lee, B., and Iorio, R. M. (2011) Triggering of the Newcastle disease virus fusion protein by a chimeric attachment protein that binds to Nipah virus receptors. *J. Biol. Chem.* **286,** 17851–17860
20. Porotto, M., Palmer, S. G., Palermo, L. M., and Moscona, A. (2012) Mechanism of fusion triggering by human parainfluenza virus type III: communication between viral glycoproteins during entry. *J. Biol. Chem.* **287,** 778–793
21. Yuan, P., Swanson, K. A., Leser, G. P., Paterson, R. G., Lamb, R. A., and Jardetzky, T. S. (2011) Structure of the Newcastle disease virus hemagglutinin-neuraminidase (HN) ectodomain reveals a four-helix bundle stalk. *Proc. Natl. Acad. Sci. U.S.A.* **108,** 14920–14925
22. Bose, S., Welch, B. D., Kors, C. A., Yuan, P., Jardetzky, T. S., and Lamb, R. A. (2011) Structure and mutagenesis of the parainfluenza virus 5 hemagglutinin-neuraminidase stalk domain reveals a four-helix bundle and the role of the stalk in fusion promotion. *J. Virol.* **85,** 12855–12866
23. Yin, H. S., Wen, X., Paterson, R. G., Lamb, R. A., and Jardetzky, T. S. (2006) Structure of the parainfluenza virus 5 F-protein in its metastable, prefusion conformation. *Nature* **439,** 38–44
24. Ludwig, K., Schade, B., Böttcher, C., Korte, T., Ohlwein, N., Baljinnyam, B., Veit, M., and Herrmann, A. (2008) Electron cryomicroscopy reveals different F1+F2 protein states in intact parainfluenza virions. *J. Virol.* **82,** 3775–3781
25. Liljeroos, L., Huiskonen, J. T., Ora, A., Susi, P., and Butcher, S. J. (2011) Electron cryotomography of measles virus reveals how matrix protein coats the ribonucleocapsid within intact virions. *Proc. Natl. Acad. Sci. U.S.A.* **108,** 18085–18090
26. Paal, T., Brindley, M. A., St. Clair, C., Prussia, A., Gaus, D., Krumm, S. A., Snyder, J. P., and Plemper, R. K. (2009) Probing the spatial organization of measles virus fusion complexes. *J. Virol.* **83,** 10480–10493
27. Schein, C. H., Zhou, B., and Braun, W. (2005) Stereophysicochemical variability plots highlight conserved antigenic areas in Flaviviruses. *Virol. J.* **2,** 40
28. Takeda, M., Takeuchi, K., Miyajima, N., Kobune, F., Ami, Y., Nagata, N., Suzaki, Y., Nagai, Y., and Tashiro, M. (2000) Recovery of pathogenic measles virus from cloned cDNA. *J. Virol.* **74,** 6643–6647
29. Cathomen, T., Buchholz, C. J., Spielhofer, P., and Cattaneo, R. (1995) Preferential initiation at the second AUG of the measles virus F mRNA: a role for the long untranslated region. *Virology* **214,** 628–632
30. Radecke, F., Spielhofer, P., Schneider, H., Kaelin, K., Huber, M., Dötsch, C., Christiansen, G., and Billeter, M. A. (1995) Rescue of measles viruses from cloned DNA. *EMBO J.* **14,** 5773–5784
31. Kurowski, M. A., and Bujnicki, J. M. (2003) GeneSilico protein structure prediction meta-server. *Nucleic Acids Res.* **31,** 3305–3307
32. Negi, S. S., Carol, A. A., Pandya, S., Braun, W., and Anderson, L. E. (2008) Co-localization of glyceraldehyde-3-phosphate dehydrogenase with ferredoxin-NADP reductase in pea leaf chloroplasts. *J. Struct. Biol.* **161,** 18–30
33. Oezguen, N., Zhou, B., Negi, S. S., Ivanciuc, O., Schein, C. H., Labesse, G., and Braun, W. (2008) Comprehensive three-dimensional modeling of allergenic proteins and amino acid composition of potential conformational IgE epitopes. *Mol. Immunol.* **45,** 3740–3747
34. Ivanciuc, O., Oezguen, N., Mathura, V. S., Schein, C. H., Xu, Y., and Braun, W. (2004) Using property-based sequence motifs and three-dimensional modeling to determine structure and functional regions of proteins. *Curr. Med. Chem.* **11,** 583–593
35. Soman, K. V., Schein, C. H., Zhu, H., and Braun, W. (2001) Homology modeling and simulations of nuclease structures. in *Nuclease Methods and Protocols* (Schein, C. H., ed) pp. 263–286, Humana Press, New York
36. Sanner, M., Widmer, A., Senn, H., and Braun, W. (1989) GEOM: a new tool for molecular modeling based on distance geometry calculations with NMR data. *J. Comput. Aided Mol. Des.* **3,** 195–210
37. Schaumann, T., Braun, W., and Wüthrich, K. (1990) The program FANTOM for energy refinement of polypeptides and proteins using a Newton-Raphson minimizer in torsion angle space. *Biopolymers* **29,** 679–694
38. Phillips, J. C., Braun, R., Wang, W., Gumbart, J., Tajkhorshid, E., Villa, E., Chipot, C., Skeel, R. D., Kalé, L., and Schulten, K. (2005) Scalable molecular dynamics with NAMD. *J. Comput. Chem.* **26,** 1781–1802
39. Fraczkiewicz, R., and Braun, W. (1998) Exact and efficient analytical calculation of the accessible surface areas and their gradients for macromolecules. *J. Comput. Chem.* **19,** 319–333
40. Negi, S. S., and Braun, W. (2007) Statistical analysis of physical-chemical properties and prediction of protein-protein interfaces. *J. Mol. Model* **13,** 1157–1167
41. Negi, S. S., Schein, C. H., Oezguen, N., Power, T. D., and Braun, W. (2007) InterProSurf: a web server for predicting interacting sites on protein surfaces. *Bioinformatics* **23,** 3397–3399
42. Mathura, V. S., Schein, C. H., and Braun, W. (2003) Identifying property-based sequence motifs in protein families and superfamilies: application to DNase-1 related endonucleases. *Bioinformatics* **19,** 1381–1390
43. Venkatarajan, M. S., and Braun, W. (2001) New quantitative descriptors of amino acids based on multidimensional scaling of a large number of

physical– chemical properties. *J. Mol. Model* **7,** 445–453
44. Buchholz, U. J., Finke, S., and Conzelmann, K. K. (1999) Generation of bovine respiratory syncytial virus (BRSV) from cDNA: BRSV NS2 is not essential for virus replication in tissue culture, and the human RSV leader region acts as a functional BRSV genome promoter. *J. Virol.* **73,** 251–259
45. Ono, N., Tatsuo, H., Hidaka, Y., Aoki, T., Minagawa, H., and Yanagi, Y. (2001) Measles viruses on throat swabs from measles patients use signaling lymphocytic activation molecule (CDw150) but not CD46 as a cellular receptor. *J. Virol.* **75,** 4399–4401
46. Cathomen, T., Naim, H. Y., and Cattaneo, R. (1998) Measles viruses with altered envelope protein cytoplasmic tails gain cell fusion competence. *J. Virol.* **72,** 1224–1234
47. Malvoisin, E., and Wild, F. (1990) Contribution of measles virus fusion protein in protective immunity: anti-F monoclonal antibodies neutralize virus infectivity and protect mice against challenge. *J. Virol.* **64,** 5160–5162
48. Sheshberadaran, H., Norrby, E., McCullough, K. C., Carpenter, W. C., and Orvell, C. (1986) The antigenic relationship between measles, canine distemper and rinderpest viruses studied with monoclonal antibodies. *J. Gen. Virol.* **67,** 1381–1392
49. Nakayama, T., Komase, K., Uzuka, R., Hoshi, A., and Okafuji, T. (2001) Leucine at position 278 of the AIK-C measles virus vaccine strain fusion protein is responsible for reduced syncytium formation. *J. Gen. Virol.* **82,** 2143–2150
50. Lee, J. K., Prussia, A., Paal, T., White, L. K., Snyder, J. P., and Plemper, R. K. (2008) Functional interaction between paramyxovirus fusion and attachment proteins. *J. Biol. Chem.* **283,** 16561–16572
51. Tsurudome, M., Ito, M., Nishio, M., Nakahashi, M., Kawano, M., Komada, H., Nosaka, T., and Ito, Y. (2011) Identification of domains on the fusion (F) protein trimer that influence the hemagglutinin-neuraminidase specificity of the f protein in mediating cell-cell fusion. *J. Virol.* **85,** 3153–3161
52. Zokarkar, A., and Lamb, R. A. (2012) The paramyxovirus fusion protein C-terminal region: mutagenesis indicates an indivisible protein unit. *J. Virol.* **86,** 2600–2609